Biochemical and Biophysical Research Communications 464 (2015) 434–440

Contents lists available at ScienceDirect

Biochemical and Biophysical Research Communications

journal homepage: www.elsevier.com/locate/ybbrc

Acid sphingomyelinase (aSMase) deficiency leads to abnormal microglia behavior and disturbed retinal function

Katharina Dannhausen [a], Marcus Karlstetter [a], Albert Caramoy [a], Cornelia Volz [b], Herbert Jägle [b], Gerhard Liebisch [c], Olaf Utermöhlen [d], Thomas Langmann [a, *]

[a] Laboratory for Experimental Immunology of the Eye, Department of Ophthalmology, University of Cologne, Cologne, Germany
[b] Department of Ophthalmology, University Hospital Regensburg, Regensburg, Germany
[c] Institute for Clinical Chemistry and Laboratory Medicine, University Hospital Regensburg, Regensburg, Germany
[d] Institute for Medical Microbiology, Immunology and Hygiene and Center for Molecular Medicine Cologne, University of Cologne, Cologne, Germany

ARTICLE INFO

Article history:
Received 10 June 2015
Accepted 21 June 2015
Available online 27 June 2015

Keywords:
Niemann-Pick disease
Acid sphingomyelinase
Microglia
Retina
Inflammation
Lipid accumulation

ABSTRACT

Mutations in the acid sphingomyelinase (aSMase) coding gene sphingomyelin phosphodiesterase 1 (*SMPD1*) cause Niemann-Pick disease (NPD) type A and B. Sphingomyelin storage in cells of the mononuclear phagocyte system cause hepatosplenomegaly and severe neurodegeneration in the brain of NPD patients. However, the effects of aSMase deficiency on retinal structure and microglial behavior have not been addressed in detail yet. Here, we demonstrate that retinas of aSMase$^{-/-}$ mice did not display overt neuronal degeneration but showed significantly reduced scotopic and photopic responses in electroretinography. *In vivo* fundus imaging of aSMase$^{-/-}$ mice showed many hyperreflective spots and staining for the retinal microglia marker Iba1 revealed massive proliferation of retinal microglia that had significantly enlarged somata. Nile red staining detected prominent phospholipid inclusions in microglia and lipid analysis showed significantly increased sphingomyelin levels in retinas of aSMase$^{-/-}$ mice. In conclusion, the aSMase-deficient mouse is the first example in which microglial lipid inclusions are directly related to a loss of retinal function.

1. Introduction

Niemann-Pick disease (NPD) type A and B are autosomal recessive inherited lysosomal storage disorders with an incidence of 0.5–1 in 100.000 [1]. The underlying genetic defects are mutations in the sphingomyelin phosphodiesterase 1 (*SPMD1*) gene that encodes acid sphingomyelinase (aSMase) [2]. The aSMase enzyme is located in the lysosomal compartment and cleaves sphingomyelin into ceramide and phosphorylcholine at a pH of 4.5–5 [3,4]. These metabolites of the sphingolipid pathway are involved in different cellular functions including proliferation, cell survival, apoptosis and inflammatory response [5]. The loss of aSMase activity leads to lipid-laden foam cells, also termed Niemann-Pick cells, which particularly affect the mononuclear phagocyte system. In patients with both NPD subtypes a cherry red macula and impairment of vision were observed [6–8]. Two different aSMase knock out mouse models have been established that mimic typical visceral clinical features of NPD types A and B [9,10]. Further studies identified an increasing amount of foam cells in the bone marrow [11] and lipid accumulation in degenerating Purkinje cells [12]. Despite these indications of neuronal degeneration in the brain, there is little information about retinal manifestations of aSMase deficiency.

Microglial cells are an important part of innate immunity in the central nervous system (CNS) [13]. In the healthy nervous tissue, microglial cells are ramified and constantly scan their microenvironment with their long protrusions, sensing disturbance in tissue homeostasis and integrity [14]. In the diseased brain and retina, reactive microglia transform into an amoeboid state with large somata and retracted protrusions and produce pro-inflammatory

* Corresponding author. Laboratory for Experimental Immunology of the Eye, Department of Ophthalmology, University of Cologne, Joseph-Stelzmann-Strasse 9, D-50931 Cologne, Germany.
E-mail address: thomas.langmann@uk-koeln.de (T. Langmann).

http://dx.doi.org/10.1016/j.bbrc.2015.06.133
0006-291X/

mediators including reactive oxygen species, nitric oxide and tumor necrosis factor α [15]. Reactive microglia do not only phagocytose damaged or dying neurons but may also attack the healthy surrounding tissue [16]. Lipids have a strong influence on the morphology and function of microglia and changes in the composition of lipid rafts lead to alterations in the cell-to-cell communication via diminished microparticle release [17]. High amounts of cholesterol also increase the expression of pro-inflammatory genes, whereas polyunsaturated fatty acids can have generally anti-inflammatory effects on microglial cells [18,19].

In this study, we analyzed the effects of aSMase deficiency on murine retinal structure and function with a focus on retinal microglia. We identified enlarged lipid-laden microglia in the aSMase$^{-/-}$ retina that were associated with pro-inflammatory marker expression. In these aSMase-deficient retinas, the microglial behavior was abnormal and electroretinography revealed a significant loss of visual function. These findings implicate that aSMase function is required to control microglia activity in the retina and to preserve retinal function.

2. Materials and methods

2.1. Animals

aSMase KO mice on C57/BL6 background were provided by Dr. Edward H Schuchman (Icahn Medical Institute, New York, USA) and were kept at a 12-h light–dark cycle. The mice were genotyped as described previously [10] and age-matched wild-type littermates served as controls. All experiments were performed in accordance with the German Law and Animal Research Guide for the Care and Use of Laboratory Animals, 2011/2013 and were in accordance with the ARVO statement for the use of animals in ophthalmology and vision Research.

2.2. Electroretinography

Mice were dark adapted for at least 12 h before the experiments and subsequently anesthetized by subcutaneous injection of ketamine and xylazine. Pupils were dilated with tropicamide eyedrops (Mydriaticum Stulln; Pharma Stulln, Germany). Silver needle electrodes served as reference (fore-head) and ground (tail) and gold wire ring electrodes as active electrodes. Corneregel (Bausch & Lomb, Berlin, Germany) was applied to keep the eye hydrated and maintain good electrical contact. ERGs were recorded using a Ganzfeld bowl (Ganzfeld QC450 SCX, Roland Consult, Brandenburg, Germany) and an amplifier & recording unit (RETI-Port, Roland Consult, Brandenburg, Germany). ERGs were recorded from both eyes simultaneously, band-pass filtered (1–300 Hz) and averaged. Single flash scotopic (dark adapted) responses to a series of ten LED-flash intensities ranging from −3.5 to 1.0 log cd.s/m^2 with an inter stimulus interval of 2 s up to 20 s for the highest intensity were recorded. Response waveforms were analyzed by means of through and peak amplitude and implicit time measurement. All analysis and plotting was carried out with R 3.1.1 and ggplot 1.0.1.

2.3. Fundus autofluorescence and Spectral Domain OCT

For the analysis of the fundus, mice were anesthetized and their eyes were treated with 1% Tropicamide and 2.5% Phenylephrine for dilation of the pupil. Infrared Reflectance (IR; λ = 815 nm) and Spectral Domain OCT (SD-OCT; λ = 870 nm, acquisition speed, 40.000 A-scans per second) were recorded at the same time for the orientation in retinal layers. Fundus Autofluorescence (FAF; excitation at λ = 488 nm, emission at λ = 500–700 nm) were used to detect autofluorescent material in the retina. All experiments were performed on a Spectralis HRA + OCT device (Heidelberg Engineering GmbH, Dossenheim, Germany).

2.4. Immunohistochemistry

Dissected eyes were fixed in 4% formaldehyde for preparation of retinal sections, retinal flat-mounts and retinal pigment epithelium/choroidal flat mounts as described previously [20]. In brief, retinal sections and flat-mounts were stained with rabbit anti-Iba1 (Wako Chemicals, Neuss, Germany), rabbit anti-TSPO (Abcam), and goat anti-GFAP (Sigma) antibodies, and counter-stained with 4′,6-diamidino-2-phenylindole (DAPI) or stained with Phalloidin-TRITC. Sections were stained with heamtoxylin/eosin and all specimens were imaged using an AxioImager.M2 plus ApoTome2 microscope (Carl Zeiss, Oberkochen, Germany).

2.5. Nile red and Filipin III staining

For detection of accumulated lipids, Iba1-stained sections were additionally incubated with Nile red diluted 1:500 in PBS for 10 min at room temperature. For detection of cholesterol, tissue was incubated for 20 min at room temperature with Filipin III (diluted 1:100 in 1x PBS) and washed three times with PBS. After staining, tissue slices were mounted in Dako fluorescent mounting medium and analysed with an AxioImager.M2 plus ApoTome2 microscope (Carl Zeiss, Oberkochen, Germany).

2.6. TUNEL assay

The *In Situ* Cell Death Detection Kit (Roche Diagnostics, Mannheim, Germany) was used to detect cell death in retinal sections and nuclei were counterstained with DAPI.

2.7. RNA isolation and quantitative real-time RT-PCR

RNA was isolated from retinas of WT and homozygous aSMase$^{-/-}$ mice with the RNeasy Micro Kit (Qiagen, Hilden, Germany). For cDNA synthesis, the RevertAid™ H Minus First strand cDNA Synthesis Kit (Thermo Scientific) was used. 50 ng of each sample was measured in triplicates. Amplifications of 50 ng cDNA were performed with an ABI7900HT machine (Applied Biosystems, Carlsbad, CA, USA) in 10 μl reaction mixtures containing 1x TaqMan Universal PCR Master Mix (Applied Biosystems), 200 nM of primers and 0.125 μl of dual-labeled UPL probe (Roche Applied Science, Basel, Switzerland). The following primer sequences and probes were used: ATP5B, forward primer 5′-ggcacaatgcaggaaagg-3′, reverse primer 5′-tcagcaggcacatagatagcc-3′, probe #77. AMWAP, forward primer 5′-tttgatcactgtggggatga-3′, reverse primer 5′-acactttctggtgaaggcttg-3′, probe #1. CD68, forward primer 5′-ctctctaaggctacaggctgct-3′, reverse primer 5′-tcacggttgcaagagaaaca-3′, probe #27. CD36, forward primer 5′-ttgaaaagtctcggacattgag-3′, reverse primer 5′-tcagatccgaacacagcgta-3′, probe #6. IL6, forward primer 5′-gatggatgctaccaaactggat-3′, reverse primer 5′-ccaggtagctatggtactccag-3′, probe #6. Measurements were performed in triplicates and results were analyzed with the ABI sequence detector software version 2.4 using the ΔΔCt method for relative quantification.

2.8. Mass spectrometric analysis of retinal lipids

Retinal samples were homogenized by bead beating in a mixture of methanol/water (1/1, v/v). Phospholipid species were quantified by electrospray ionization tandem mass spectrometry

(ESI-MS/MS) using the analytical setup and chloroform extraction described previously [21]. A precursor ion scan of mass/charge (*m/z*) 184, specific for phosphocholine-containing lipids, including (lyso)phosphatidylcholine, sphingomyelin. Sphingosine-based ceramides were analyzed using a fragment ion of *m/z* 264 [22]. Correction of isotopic overlap of lipid species and data analysis were performed using self-programmed Excel macros for all lipid classes as previously described [21]. Lipid species were annotated according to the LipidomicNet proposal for shorthand notation of lipid structures derived from mass spectrometry [23]. Sphingomyelin species were assigned based on the assumption of a sphingoid base with two hydroxyl groups.

2.9. Statistical analysis

For the analysis of cell body size and number of microglial cells Iba1-stained flat mounts were quantified. Ten images at different locations were made at 20-fold magnification for each flat mount. Microglial cell body size was determined using the Zen Imaging Software (Zeiss). A two-tailed Student's t-test was used when two groups were compared, and ANOVA with post-hoc Bonferroni analysis was used when multiple groups were compared. The null hypothesis was rejected at $p < 0.05$.

3. Results

3.1. Retinas from aSMase-deficient mice show no overt signs of neuronal degeneration

As vision problems were described in NPD type A and B patients we first investigated if aSMase deficiency leads to overt neuronal degeneration in the retina. Therefore, cryosections from age-matched wild-type and aSMase$^{-/-}$ mice were stained with hematoxylin and eosin. Analysis of retinal sections from wild-type and aSMase$^{-/-}$ mice at one, four, and six months of age indicated no gross change in retinal structure and thickness (Fig. S1). Furthermore, the number of TUNEL positive cells as indicator for apoptotic cell death was similar in five month old aSMase-deficient retinas compared to wild-type animals (Fig. S2). These data indicate that aSMase deficiency does not lead to a strong retinal degenerative phenotype that is present in the first months of life.

3.2. aSMase$^{-/-}$ mice show impaired retinal function

We next performed dark-adapted (scotopic) and photopic ERG measurements as an independent measure of retinal function. Rod photoreceptor function (a-wave) and inner retinal function

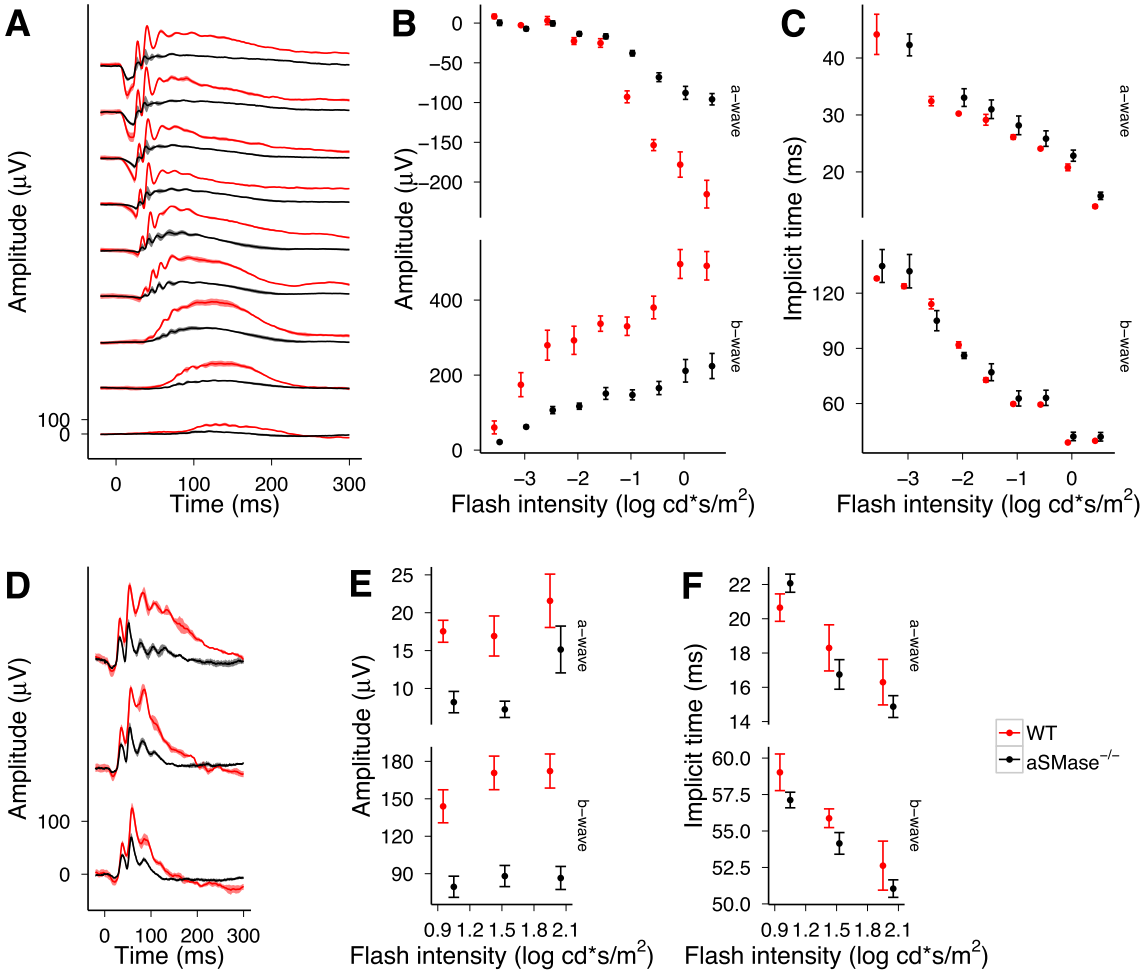

Fig. 1. Scotopic and photopic electroretinograms in aSMase-deficient mice. (A–C) Response waveforms obtained under scotopic (dark adapted) conditions and peak amplitude as well as implicit time analysis of the initial trough (a-wave) and the maximum peak (b-wave). (D–F) Response waveforms and analysis obtained under light adapted condition.

dominated by the contribution of the bipolar cells (b-wave) were both determined for four month old wild-type and aSMase$^{-/-}$ mice (Fig. 1). There was a significant reduction of a-wave amplitude and a proportional reduction of the b-wave amplitude consistent with a photoreceptor dominated or all retinal layer involving function loss (Fig. 1A, B). Similar results were found under photopic conditions (Fig. 1D, E). There was no difference in the response implicit time for both conditions (Fig. 1C, F).

3.3. Reactive microgliosis in aSMase$^{-/-}$ retinas

As aSMase deficiency affects cells of the mononuclear phagocyte system, we then analyzed the localization and morphology of retinal microglial cells by immunostaining with the marker Iba1 (Fig. 2). aSMase-deficient microglial cells were localized in the plexiform layers and showed a normal distribution. However, these cells exhibited an altered morphology with enlarged somata compared to wild-type microglia. Since the increase of cell body size is a hallmark of microglia reactivity we stained with an antibody against translocator protein (18 kDa) (TSPO) [20]. This staining demonstrated an increase in TSPO-positive cells in the aSMase$^{-/-}$ retina compared to wild-type controls, which was particularly pronounced in six months old animals (Fig. S3). Staining of retinal sections with an anti-GFAP antibody did not reveal significant Müller cell gliosis in the aSMase$^{-/-}$ retina compared to wild-type controls (Fig. S4). These data indicate an isolated microgliosis without indications of Müller cell reactivity.

3.4. Increased expression of microglia-specific and pro-inflammatory transcripts in aSMase-deficient retinas

We next wanted to clarify if these reactive microglia in aSMase$^{-/-}$ retinas also express higher levels of myeloid-specific and pro-inflammatory markers using quantitative real-time RT-PCR. CD68, a general marker that reflects the presence of microglia was significantly increased in retinal RNA fractions of young aSMase$^{-/-}$ animals (Fig. S5A). Moreover, AMWAP (activated microglia/macrophage whey acidic protein), a marker of pro-inflammatory microglia and macrophages was also upregulated in aSMase-deficient retinas (Fig. S5B). These data reveal that the microglia phenotype in aSMase$^{-/-}$ retinas is very like reactive.

3.5. Proliferation and increased cell body size of aSMase-deficient microglial cells

To further characterize the retinal microglia morphology and behavior, Iba1-stained flat mounts of aSMase-deficient and wild-type retinas were compared over time. An altered morphology and higher density of microglia was identified at all time points in aSMase$^{-/-}$ retinas compared to wild-type controls (Fig. 3A, B). Microscopic quantification showed a significantly increased number of microglial cells in aSMase-deficient retinas of all ages compared to wild-type animals (Fig. 3B). When analyzing microglial morphology in detail, aSMase-deficient microglia were ramified with long and branched protrusions and showed a regular spatial distribution (Fig. 3A). However, these cells had a strongly enlarged cell body size at all ages when compared to controls (Fig. 3C).

3.6. Increased number of hyperreflective spots in aSMase-deficient retinas

We next performed *in vivo* fundus autofluorescence imaging of aSMase-deficient mice and wild-type controls. In this analysis, some autofluorescent hyperreflective spots became visible in wild-type mice but a strongly increased number of these spots was observed in aSMase-deficient mice (Fig. S6, top panels). A direct comparison of these fundus images with Iba1-stained retinal flat mounts of the same eyes showed a good correlation with the microglia number and patterning (Fig. S6, bottom panels). Moreover, an increase in microglial number and abnormal morphology was not only observed in the inner retina of aSMase-deficient mice but was also seen at the level of the retinal pigment epithelium (RPE) (Fig. S7). The RPE of wild-type mice was very scarcely occupied by retina microglia (Fig. S7. *left panel*). In contrast, the RPE layer of aSMase-deficient mice was densely covered by microglia (Fig. S7, *right panel*).

3.7. Accumulation of sphingolipid-rich phospholipids but not of cholesterol in aSMase-deficient microglial cells

We were next interested whether aSMase-deficient abnormal retinal microglial cells contain lysosomal phospholipid inclusions. Therefore, retinal sections were stained with the fluorescent dye Nile red, which is commonly used to detect sphingomyelin-rich phospholipids in NPD cells [24]. The comparison between Iba1- and Nile red-stained sections of wild-type and aSMase-deficient retinas clearly showed an accumulation of orange fluorescence signal in aSMase-deficient Iba1-positive cell bodies whereas no Nile red staining was detectable in somata of wild-type microglial cells (Fig. 4). Of note, staining with the cholesterol-specific dye

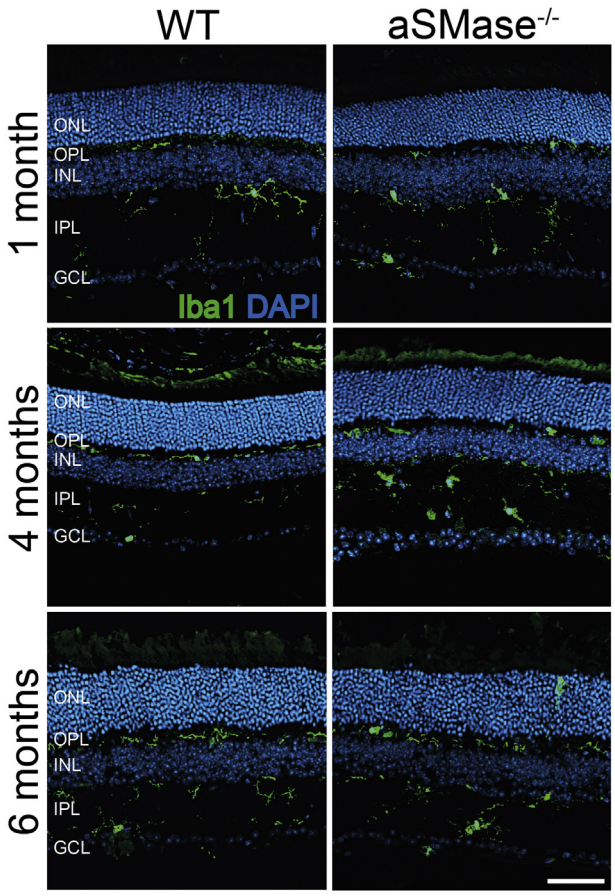

Fig. 2. Normal distribution but abnormal morphology of microglial cells in aSMase-deficient retinas. Iba1 staining of microglial cells in aSMase retinas and wild-type controls at different ages. Scale bar: 50 μm Iba1, ionized calcium binding adaptor molecule 1; ONL, outer nuclear layer; OPL, outer plexiform layer; INL, inner nuclear layer; IPL, inner plexiform layer; GCL, ganglion cell layer.

Filipin III showed an even distribution within the retina and no obvious accumulation of cholesterol in Iba1 positive cells in aSMase-deficient mice (Fig. S8). Finally, we could verify that sphingomyelin levels were strongly increased in retinal phospholipids of aSMase$^{-/-}$ mice compared to wild-type animals (Fig. S9A). Of note, there was no significant difference in total ceramide levels between aSMase$^{-/-}$ mice and wild-type controls (Fig. S9B).

4. Discussion

A few studies describe visual impairment, vision loss and a cherry red macula in patients with aSMase deficiency [2,25,26]. In this study, aSMase$^{-/-}$ mice at different ages showed no significant thinning of the retinal layers and no overt cell death. In line with this, no retinal degeneration was observed in post mortem specimens of NPD type B patients [8]. The reduced ERG amplitudes with normal implicit times presented here are consistent with a dysfunction without degeneration. Even though there is no evidence for a photoreceptor dysfunction in NPD type B, some patients exhibit macular halos, a white ring of lipid-laden neurons [27] that are usually not associated with visual impairment [28].

The increased expression of the microglia-specific reactivity markers TSPO, AMWAP and CD68 but the concomitant low expression of the gliosis marker GFAP indicates that the loss of aSMase leads to an unconventional gliosis in aSMase-deficient mice. The enlarged microglial somata in aSMase-deficient retinas can be related to the accumulation of lipids and Nile red-staining showed that the storage material seen in microglia is rich in sphingomyelin as previously reported for other tissues, cells, and body fluids [29]. Of note, there was no accumulation of cholesterol that indicates selective lipid storage corresponding to lipid-laden cells that are characteristic for Niemann-Pick type A and B [30].

The microglial cells in aSMase-deficient retinas displayed a unique phenotype with long and branched protrusions but enlarged cell bodies and expression of pro-inflammatory mediators. On the one hand microglial cells could display characteristics of lipotoxicity, which is known from macrophages which actively secrete pro-inflammatory cytokines [30]. On the other hand aSMase-deficient microglial cells have a more ramified morphology and no cell death surrounding these cells was observed. This lack of neurotoxicity could potentially arise from two known pathways. Accumulated lipids may activate peroxisome proliferator activator receptor γ (PPARγ), which usually leads to a decrease in the expression of pro-inflammatory mediators and inhibits NFκB activity [31]. Another pathway could be mediated by sphingosine and ceramide. Ceramide and especially sphingosine-1-phosphate (S1P) have an important function as second messengers and are involved in cell proliferation and regulation of apoptosis [32]. While an excess of ceramide can lead to cell death, S1P has cell survival-promoting activity. Our lipid analysis did not reveal major changes in ceramide levels, which could be expected by aSMase deficiency. An explanation could be that ceramide is not only generated from sphingomyelin via aSMase activity but also synthesized *de novo* in the endoplasmatic reticulum independently from aSMase. S1P, which is metabolized from ceramide, can also inhibit aSMase activity which could then trigger proliferation and survival of cells. The interaction of these pathways could be a reason for the higher density of lipid-laden microglial cells and

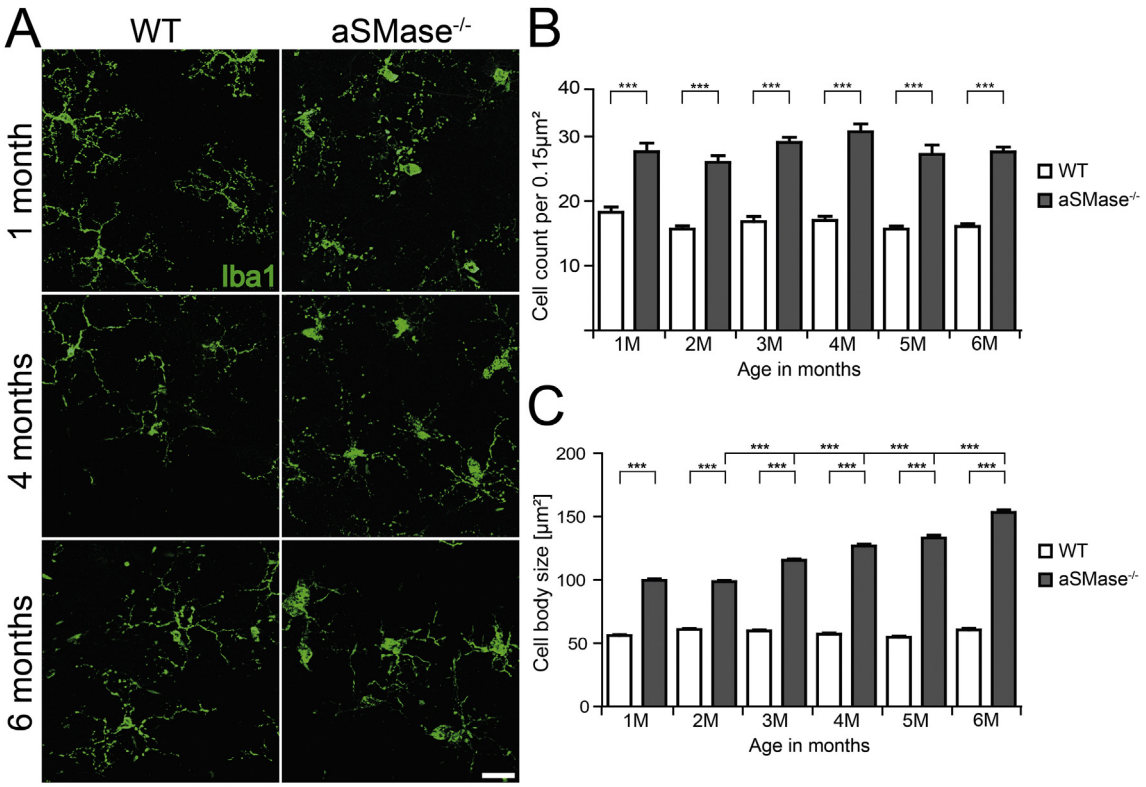

Fig. 3. Abnormal morphology and increased number of Iba1-positive microglial cells in aSMase-deficient retinas. (A) Retinal flat mount images of Iba1-stained microglial cells show an altered morphology of aSMase-deficient microglia compared to controls. Scale bar: 20 µm. (B) Quantification of microglial cells in aSMase-deficient mice compared to age-matched control mice showed a significantly increased number of microglia in retinas from aSMase-deficient animals. (C) Quantification of microglial size in aSMase-deficient mice compared to age-matched controls showed a significant enlargement of microglial cell body size in retinas with aSMase deficiency. Data show mean ± SD (n = 10 frames/group). $^{*}P < 0.05$; $^{**}P < 0,01$; $^{***}P < 0.001$.

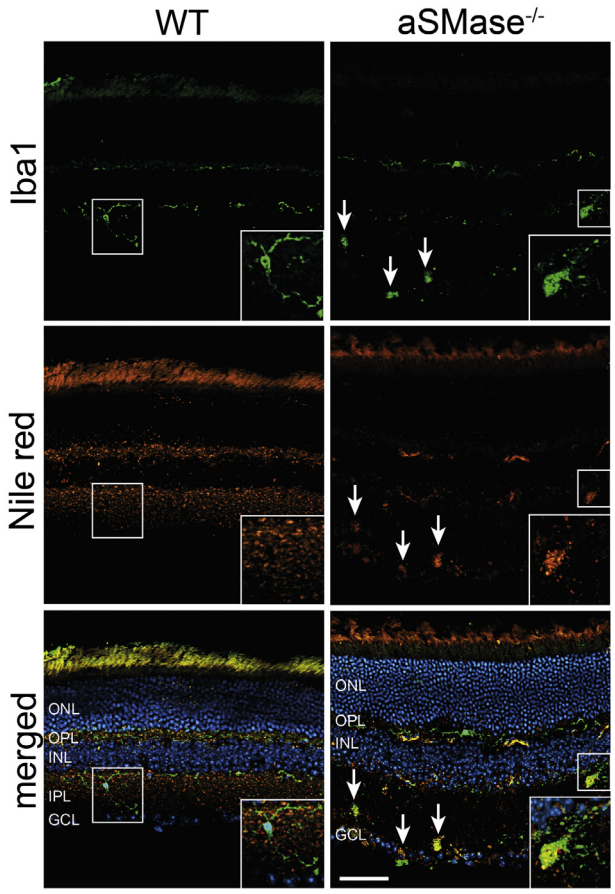

Fig. 4. Detection of lysosomal phospholipid accumulation in aSMase-deficient retinas. Co-staining of retinal sections from aSMase$^{-/-}$ and wild-type mice with Nile red and Iba1 detects orange-fluorescent lipid deposits within enlarged microglial cells in aSMase-deficient retinas. Scale bar: 50 μm. ONL, outer nuclear layer; OPL, outer plexiform layer; INL, inner nuclear layer; IPL, inner plexiform layer; GCL, ganglion cell layer. (For interpretation of the references to colour in this figure legend, the reader is referred to the web version of this article.)

their partially ramified status in aSMase-deficient retinas. How these mechanisms act on a molecular level within retinal microglia is a key question that remains to be investigated in the future.

Conflict of interest

All authors declare no conflict of interests.

Acknowledgements

The authors thank Ulrike Karow for her excellent technical assistance. This work was supported by the DFG (LA1203/6-2 and LA1203/9-1), the Hans und Marlies Stock-Foundation, the Pro Retina Foundation, the Marga und Walter Boll foundation, and the Bayer Graduate Program in Pharmacology.

Appendix A. Supplementary data

Supplementary data related to this article can be found at http://dx.doi.org/10.1016/j.bbrc.2015.06.133.

Transparency document

Transparency document related to this article can be found online at http://dx.doi.org/10.1016/j.bbrc.2015.06.133.

References

[1] E.H. Schuchman, The pathogenesis and treatment of acid sphingomyelinase-deficient Niemann-Pick disease, J. Inherit. Metab. Dis. 30 (2007) 654–663.
[2] T. Kolter, K. Sandhoff, Sphingolipid metabolism diseases, Biochimica Biophys0. Acta 1758 (2006) 2057–2079.
[3] R.O. Brady, J.N. Kanfer, M.B. Mock, D.S. Fredrickson, The metabolism of sphingomyelin. II. Evidence of an enzymatic deficiency in Niemann-Pick diseae, Proc. Natl. Acad. Sci. U S A 55 (1966) 366–369.
[4] R.W. Jenkins, D. Canals, Y.A. Hannun, Roles and regulation of secretory and lysosomal acid sphingomyelinase, Cell. Signal 21 (2009) 836–846.
[5] Y.A. Hannun, L.M. Obeid, Principles of bioactive lipid signalling: lessons from sphingolipids, Nat. Rev. Mol. Cell. Biol. 9 (2008) 139–150.
[6] W. Sperl, G. Bart, M.T. Vanier, H. Christomanou, I. Baldissera, E. Steichen-Gersdorf, E. Paschke, A family with visceral course of Niemann-Pick disease, macular halo syndrome and low sphingomyelin degradation rate, J. Inherit. Metab. Dis. 17 (1994) 93–103.
[7] M.M. McGovern, T. Pohl-Worgall, R.J. Deckelbaum, W. Simpson, D. Mendelson, R.J. Desnick, E.H. Schuchman, M.P. Wasserstein, Lipid abnormalities in children with types A and B Niemann-Pick disease, J. Pediatr. 145 (2004) 77–81.
[8] M.M. McGovern, M.P. Wasserstein, A. Aron, R.J. Desnick, E.H. Schuchman, S.E. Brodie, Ocular manifestations of Niemann-Pick disease type B, Ophthalmology 111 (2004) 1424–1427.
[9] B. Otterbach, W. Stoffel, Acid sphingomyelinase-deficient mice mimic the neurovisceral form of human lysosomal storage disease (Niemann-Pick disease), Cell 81 (1995) 1053–1061.
[10] K. Horinouchi, S. Erlich, D.P. Perl, K. Ferlinz, C.L. Bisgaier, K. Sandhoff, R.J. Desnick, C.L. Stewart, E.H. Schuchman, Acid sphingomyelinase deficient mice: a model of types A and B Niemann-Pick disease, Nat. Genet. 10 (1995) 288–293.
[11] T.A. Kuemmel, J. Thiele, R. Schroeder, W. Stoffel, Pathology of visceral organs and bone marrow in an acid sphingomyelinase deficient knock-out mouse line, mimicking human Niemann-Pick disease type A. A light and electron microscopic study, Pathol. Res. Pract. 193 (1997) 663–671.
[12] T.A. Kuemmel, R. Schroeder, W. Stoffel, Light and electron microscopic analysis of the central and peripheral nervous systems of acid sphingomyelinase-deficient mice resulting from gene targeting, J. Neuropathol. Exp. Neurol. 56 (1997) 171–179.
[13] H. Kettenmann, U.K. Hanisch, M. Noda, A. Verkhratsky, Physiology of microglia, Physiol. Rev. 91 (2011) 461–553.
[14] A. Nimmerjahn, F. Kirchhoff, F. Helmchen, Resting microglial cells are highly dynamic surveillants of brain parenchyma in vivo, Science 308 (2005) 1314–1318.
[15] M. Karlstetter, R. Scholz, M. Rutar, W.T. Wong, J.M. Provis, T. Langmann, Retinal microglia: just bystander or target for therapy? Prog. Retin. Eye Res. 45 (2015) 30–57.
[16] S. Thanos, S. Moore, Y. Hong, Retinal microglia, Prog. Retin. Eye Res. 15 (1996) 331–361.
[17] F. Antonucci, E. Turola, L. Riganti, M. Caleo, M. Gabrielli, C. Perrotta, L. Novellino, E. Clementi, P. Giussani, P. Viani, M. Matteoli, C. Verderio, Microvesicles released from microglia stimulate synaptic activity via enhanced sphingolipid metabolism, EMBO J. 31 (2012) 1231–1240.
[18] M. Indaram, W. Ma, L. Zhao, R.N. Fariss, I.R. Rodriguez, W.T. Wong, 7-Ketocholesterol increases retinal microglial migration, activation, and angiogenicity: a potential pathogenic mechanism underlying age-related macular degeneration, Sci. Rep. 5 (2015) 9144.
[19] S. Ebert, K. Weigelt, Y. Walczak, W. Drobnik, R. Mauerer, D.A. Hume, B.H. Weber, T. Langmann, Docosahexaenoic acid attenuates microglial activation and delays early retinal degeneration, J. Neurochem. 110 (2009) 1863–1875.
[20] M. Karlstetter, C. Nothdurfter, A. Aslanidis, K. Moeller, F. Horn, R. Scholz, H. Neumann, B.H. Weber, R. Rupprecht, T. Langmann, Translocator protein (18 kDa) (TSPO) is expressed in reactive retinal microglia and modulates microglial inflammation and phagocytosis, J. Neuroinflammation 11 (2014) 3.
[21] G. Liebisch, B. Lieser, J. Rathenberg, W. Drobnik, G. Schmitz, High-throughput quantification of phosphatidylcholine and sphingomyelin by electrospray ionization tandem mass spectrometry coupled with isotope correction algorithm, Biochim. Biophys. Acta 1686 (2004) 108–117.
[22] G. Liebisch, W. Drobnik, M. Reil, B. Trumbach, R. Arnecke, B. Olgemoller, A. Roscher, G. Schmitz, Quantitative measurement of different ceramide species from crude cellular extracts by electrospray ionization tandem mass spectrometry (ESI-MS/MS), J. Lipid Res. 40 (1999) 1539–1546.
[23] G. Liebisch, J.A. Vizcaino, H. Kofeler, M. Trotzmuller, W.J. Griffiths, G. Schmitz, F. Spener, M.J. Wakelam, Shorthand notation for lipid structures derived from mass spectrometry, J. Lipid Res. 54 (2013) 1523–1530.
[24] W.J. Brown, T.R. Sullivan, P. Greenspan, Nile red staining of lysosomal phospholipid inclusions, Histochemistry 97 (1992) 349–354.
[25] M.P. Wasserstein, A. Aron, S.E. Brodie, C. Simonaro, R.J. Desnick, M.M. McGovern, Acid sphingomyelinase deficiency: prevalence and characterization of an intermediate phenotype of Niemann-Pick disease, J. Pediatr. 149 (2006) 554–559.
[26] R.M. Robb, T. Kuwabara, The ocular pathology of type A Niemann-Pick disease. A light and electron microscopic study, Invest. Ophthalmol. 12 (1973) 366–377.

[27] M.R. Filling-Katz, J.K. Fink, M.B. Gorin, R. Caruso, J.B. Carl, E.J. Fitzgibbon, N.W. Barton, N.N. Katz, Ophthalmologic manifestations of type B Niemann-Pick diseases, Metab. Pediatr. Syst. Ophthalmol. 15 (1992) 16–20.
[28] C. Kim, J. Jeong, H.G. Yu, Diagnostic and predictive methods for a Niemann-Pick disease type B patient with ocular involvement, J. Inherit. Metab. Dis. 33 (2010) 633–634.
[29] X. He, F. Chen, M.M. McGovern, E.H. Schuchman, A fluorescence-based, high-throughput sphingomyelin assay for the analysis of Niemann-Pick disease and other disorders of sphingomyelin metabolism, Anal. Biochem. 306 (2002) 115–123.
[30] J.P. Truman, M.M. Al Gadban, K.J. Smith, S.M. Hammad, Acid sphingomyelinase in macrophage biology, Cell. Mol. Life Sci. 68 (2011) 3293–3305.
[31] M. Ricote, A.C. Li, T.M. Willson, C.J. Kelly, C.K. Glass, The peroxisome proliferator-activated receptor-gamma is a negative regulator of macrophage activation, Nature 391 (1998) 79–82.
[32] D. Canals, D.M. Perry, R.W. Jenkins, Y.A. Hannun, Drug targeting of sphingolipid metabolism: sphingomyelinases and ceramidases, Br. J. Pharmacol. 163 (2011) 694–712.